



Article

Initial Stages of Al-AM60-Modified Surface of Magnesium Alloy Activity Exposed to Simulated Marine Environment

Gerardo Sánchez D, Lucien Veleva * D and Eduardo Flores D

Applied Physics Department, Center for Research and Advanced Studies (Cinvestav-Merida), Merida 97310, Mexico; gerardo.sanchezs@cinvestav.mx (G.S.); eduardo.flores@cinvestav.mx (E.F.)

* Correspondence: veleva@cinvestav.mx; Tel.: +52-999-9429477

Abstract: The surface of AM60 magnesium alloy was modified with Al-nanocoating ~65.62 nm, using DC magnetron sputtering to enhance its resistance to degradation under aggressive marine ambience. The sputtered Al film showed adhesion to the α -Mg matrix, covering the dispersed particles of the β -Mg₁₇Al₁₂ secondary phase. The aluminum nanofilm was composed of (111) and (200) crystal planes of metallic aluminum (Al^0) and Al_2O_3 (Al^{3+}). After 30 days of immersion in a simulated marine environment (SME, pH 7.8), the Al-AM60 maintained a lower alkaline value (pH~8.13) of SME than that of uncoated AM60, attributed to α -Mg electrochemical oxidation to Al₂O₃ and its posterior dissolution, consuming OH⁻ ions. Consequently, the concentration of the released Mg²⁺ ions from the Al-AM60 surface was reduced ~2.3 times (~15 mg L^{-1}). The Rp (polarization resistance), as inversely proportional to the corrosion current, was extracted from the EIS impedance data fitted to an equivalent electrical circuit. After 30 days in SME solution, the Rp value of the Al-AM60 modified surface was ~3.5 times higher than that of AM60 (~15.46 k Ω cm²), confirming that the sputtered aluminum nano-deposit layer can hinder the corrosion process. These reported findings indicated that sputtered Al nano-coatings can mitigate the surface degradation of Mg-Al alloys in saline aggressive marine environments.

Keywords: surface modification; magnesium-aluminum alloy; aluminum coating; magnetron sputtering; corrosion resistance; electrochemical tests; marine environment



Academic Editors: Jordan Todorov Maximov and Galya Velikova Duncheva

Received: 3 May 2025 Revised: 23 May 2025 Accepted: 27 May 2025 Published: 30 May 2025

Citation: Sánchez, G.; Veleva, L.; Flores, E. Initial Stages of Al-AM60-Modified Surface of Magnesium Alloy Activity Exposed to Simulated Marine Environment. Coatings 2025, 15, 661. https:// doi.org/10.3390/coatings15060661

Copyright: © 2025 by the authors. Licensee MDPI, Basel, Switzerland. This article is an open access article distributed under the terms and conditions of the Creative Commons Attribution (CC BY) license (https://creativecommons.org/licenses/by/4.0/).

1. Introduction

Magnesium alloys are among the lightest structural materials, offering an excellent balance of mechanical properties, including high specific strength and stiffness, superior damping capacity, high dimensional stability, and good machinability [1–5]. Due to these advantages, magnesium alloys are highly desirable for applications in the automotive, aerospace, communication and computer industries [6–14].

Mg-Al alloys are the most used material in the transport, electronics, and sports industries to produce lightweight elements [15,16], improving mechanical, fabrication and welding characteristics and reducing the production cost as compared to pure metal. Besides the excellent physical and mechanical properties of these alloys, the weight reduction makes them ideal materials for automotive and aerospace applications. A commercial magnesium-aluminum alloy-extruded AM60 was selected as it is used in the manufacture of high-pressure die castings for the automotive industry. In contact with air oxygen, a thin, stable passive layer of aluminum oxide (Al $_2$ O $_3$) is formed on Mg-Al alloy surface, which provides a decrease in the Mg-matrix corrosion rate, giving it corrosion resistance. However, in the industrial atmosphere (acid rain) or marine environment (rich in chloride

Coatings 2025, 15, 661 2 of 13

ions), the corrosion layer of insoluble $Mg(OH)_2$ is transformed to soluble $MgCl_2$, and the Mg-matrix suffers degradation, limiting certain Mg alloy applications, particularly in the automotive industry [17–24]. Previous investigations have revealed that in chloride-polluted atmospheric environments, the corrosion rate of AM50 increases up to 250 μg cm² as a function of NaCl concentration [19]. It has been reported that the corrosion layer of AM50 presents two parts: $MgO/Mg(OH)_2$ (outer layer) and Al_2O_3 (thin inner layer) [25]. However, the corrosion layers do not have the same composition when the corroded areas possess lower Al-contents (2–3% wt.).

To improve the corrosion performance of Mg alloys, surface modification techniques have been proposed as alternative strategies, such as anodizing treatment [26,27], Al-Al₂O₃ composite [28], coatings by plasma electrolytic oxidation and sol-gel technique [29], microarc oxidation [30], magnetron-sputtered nano-hydroxyapatite coating [31], fluorocarbon polymeric film [32], aluminum electroplating [33], polymer-graphene oxide as self-healing monomolecular films [34], and Mg-Al-layered double hydroxide [35].

The selection of coating material plays a crucial role in ensuring adequate anti-corrosion protection, with most effectively delaying corrosion damage. The surface of the obtained coating must be uniform and strongly adhered to the material substrate [36,37]. The smaller the difference between the electrochemical potentials of the always active Mg matrix (anode) and the applied coating (more noble in potential), the better the anti-corrosive protection for the substrate material [38,39]. Such galvanic cells of two metals closer in potentials will provide smaller input for the progress in the corrosion process. Among the available options, aluminum coatings have been employed for corrosion protection on various metal surfaces, mainly because their air-formed passive Al₂O₃ layer acts as an efficient barrier against aggressive environments [40–43]. However, in the presence of air oxygen, a layer of MgO is formed on the magnesium alloy surface, which reduces the adhesion strength of the coating and thus negatively impacting its protective effectiveness. The introduction of an interlayer metallic element between the substrate and the coating may potentially extend its service life [44].

In Mexico there are around 11,000 km of marine-coastal areas, the aggressive atmosphere of which leads to accelerated corrosion of transport vehicle metal structures, shorting their service life. To improve the corrosion resistance of AM60 alloy, exposed to simulated marine ambience, the surface has been modified in different ways: by reinforcement with aluminum nitride (AM60-AIN nanocomposite) [45], polystyrene- ZrO_2 coating [46], vanadium and V_2O_5 sputtered deposit [47], and by electroless ZnO coating [48]. The initial stages of AM60-modified alloy have been monitored by applying different techniques.

The comparison of the AM60-Vanadium (~450 nm) and AM60-V $_2$ O $_3$ (~350 nm) surface corrosion activities showed that the AM60-V presented a lower concentration of Mg $^{2+}$ ion release (lower degradation rate), which was attributed to the possible intercalation of these cations into the conductive tunnels of V $_2$ O $_3$, as the main component of the vanadium sputtered deposit. V $_2$ O $_3$, oxide has been reported as a material for high-capacitive energy storage and in this way, the V-deposit provided longer partial protection for the AM60 surface (Mg matrix) from localized pitting attacks.

The present study aims to explore a new approach to improve the corrosion resistance of the AM60 surface through an Al-metallic deposit achieved by non-reactive DC magnetron sputtering. The electrochemical activity of AM60 and Al-AM60 were compared, after immersion over 30 days in a simulated marine ambience (SME). The variation in SME solution pH and the concentration of released Mg²⁺ ions were monitored, to correlate with the change in free corrosion potential value (OCP). The surface microstructural characteristics were analyzed using scanning electron microscopy coupled with energy-dispersive spectroscopy (SEM-EDS), X-ray photoelectron spectroscopy (XPS), and X-ray diffraction

Coatings 2025, 15, 661 3 of 13

(XRD). The electrochemical impedance spectroscopy (EIS) was carried out to provide the characteristic parameters of the alloy-electrolyte (SME) interface.

2. Materials and Methods

2.1. Sample Preparation and Model Solution

Samples of AM60 (6.0% Al, 0.2%–0.4% Mn) magnesium alloy were extruded in rod shape with a 10 mm diameter and cut into ~ 1 mm thickness. The AM60 alloy was provided by the Magnesium Innovation Center in Bottrop, Germany. The preparation of samples involved grinding with silicon carbide (SiC) sandpaper of up to 1000 grit, followed by ultrasonic cleaning in ethanol for 5 min and drying at room temperature. The SME marine-coastal model solution was composed of analytical-grade Aldrich reagents, specifically 5.84 g L $^{-1}$ NaCl, 4.09 g L $^{-1}$ Na $_2$ SO4, and 0.20 g L $^{-1}$ NaHCO3, dissolved in ultrapure deionized water (18.2 M Ω cm). The pH solution of the as-formed solution was 7.80 (PH60 Premium Line pH tester, Apera Instruments, LLC., Columbus, OH, USA).

2.2. Coating Deposition

Al-deposition on the AM60 Mg-Al alloy surface was performed through DC magnetron sputtering (Figure 1). The vacuum chamber achieved a base pressure of 1×10^{-5} Torr. Argon (Ar) was used to generate an Ar plasma at a constant working pressure of 4 mTorr. The Al-film was obtained by sputtering the Al target (99.5%) for 5 min at 100 W power and a temperature of about 45 °C. The working distance was maintained at 60 mm, and the deposition rate was ~13 nm min⁻¹.

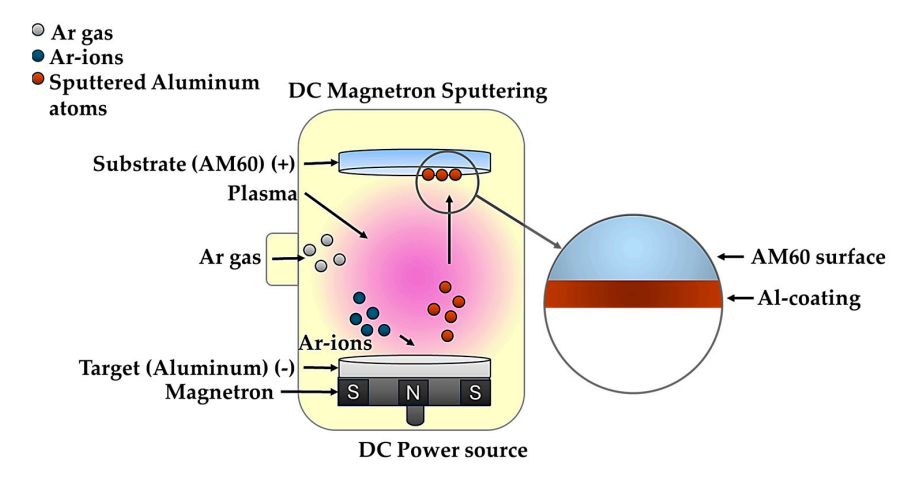


Figure 1. A schematic illustration of the DC magnetron sputtering deposition process.

2.3. Surface Characterization and Immersion Test

The morphology and composition of the uncoated AM60 and Al-AM60 surfaces were characterized before and after the immersion test in SME, using scanning electron microscopy coupled with energy dispersive X-ray spectrometry (SEM-EDS, XL-30 ESEM-JEOL JSM-7600F, JEOL Ltd., Tokyo, Japan). X-ray diffraction (XRD) patterns (Siemens D-5000 diffractometer, Munich, Germany, 20 at 34 kV and 25 mA/CuK), configured in grazing incidence (penetration depth of about 2 μ c), were used for defect metallic and oxide crystal structures. Additionally, X-ray photoelectron spectroscopy (XPS, K-Alpha Surface Analyzer, Thermo Scientific, Waltham, MA, USA) was carried out at various erosion stages of the sample surface, achieved by a scanning Ar-ion gun. The binding energies of the XPS spectra were normalized to the C1s emission peak at 284.8 eV to ensure consistency in the measurements. Cross-sectional SEM imaging was performed on a fractured surface to verify the uniformity of the Al-deposit and estimate its thickness.

Coatings 2025, 15, 661 4 of 13

Immersion tests were conducted in 20 mL of SME for different periods of 1, 7, 10, 15, and 30 days (in triplicate), following the procedure of ASTM G31-12a standard [49]. Throughout the immersion process, the SME temperature was maintained at room temperature (~22 °C), and the pH of the solution was monitored. The residual solutions were collected in separate containers for further analysis by photometry (HI83200, Hanna Instruments, Woonsocket, RI, USA) to quantify the concentration of Mg-released ions. The withdrawn metal samples were carefully rinsed with deionized water and air-dried at room temperature for their further surface characterization.

2.4. Electrochemical Characterization

The tests involved monitoring the variation of open circuit potential (OCP, free corrosion potential) over time during the immersion of uncoated AM60 and Al-AM60 surfaces. The samples (working electrodes), with a working area of $0.78~\rm cm^2$, were immersed in 20 mL of SME solution, and measurements were conducted using a three-electrode cell configuration. A saturated calomel electrode (SCE, CH Instruments Inc., Austing, TX, USA) was used as the reference electrode, while a Pt-mesh (Alfa Aesar, Ward Hill, MA, USA) served as the counter electrode. The electrodes were connected to an Interface-1000E potentiostat/galvanostat/ZRA system (Gamry Instruments, Philadelphia, PA, USA) to record the Electrochemical Impedance Spectroscopy (EIS) Nyquist diagrams, obtained with a perturbation amplitude of $\pm 10~\rm mV$ (vs. stabilized OCP after 2 h) over a frequency range of 100 kHz to 10 mHz. The EIS data were analyzed (V.7.1 Gamry Echem Analyst software, Gamry Instruments, Inc.) and fitted to electrical equivalent circuit to determine the characteristics parameters of the metal-electrolyte interface.

3. Results

3.1. X-Ray Diffraction Analysis

The X-ray diffraction (XRD) patterns for the AM60 alloy and Al-AM60 systems are shown in Figure 2. On the uncoated AM60 surface (Figure 2a) the XRD spectra suggested the presence of the α -Mg (majority phase of the matrix, JCPDS 01-077-6797) as well as the secondary phase of β -Mg₁₇Al₁₂ (JCPDS 01-076-2702) in a very low intensity, previously reported for Mg-Al alloys [50–52]. On the Al-AM60 surface (Figure 2b) the XRD signals were dependent on the thickness of the sputtered thin Al-film and the diffracted signals originated mainly from the underlying Mg-based alloy, reducing the relative intensity of aluminum peaks. The slight diffraction peaks observed at $2\theta \approx 38.44^\circ$ and 44.61° correspond to (111) and (200) crystal planes of α -metallic aluminum (JCPDS 00-004-0787), previously reported in the literature [53,54], confirming the presence of Al-deposit. The diffraction pattern of β -Mg₁₇Al₁₂ secondary phase was still detectable.

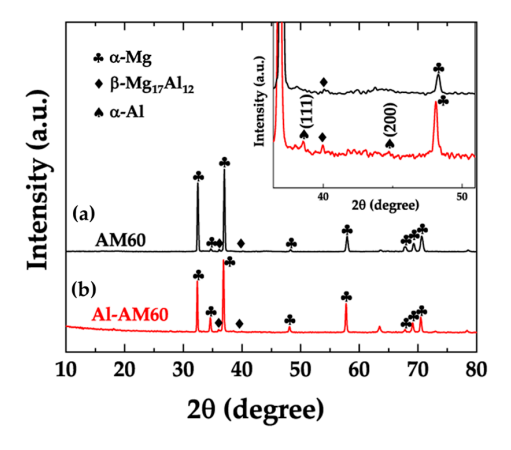


Figure 2. XRD patterns of (a) bare AM60 and (b) Al-AM60 surface.

Coatings 2025, 15, 661 5 of 13

3.2. SEM-EDS Characterization

The SEM micrographs (Figure 3) illustrate the morphological differences between the uncoated AM60 surface (Figure 3a) and that of the Al-AM60 (Figure 3b), modified through Al-sputtering. The SEM image of the uncoated AM60 substrate showed the multiple dispersed clusters of white color on the Mg-matrix, where EDS analysis (Table 1) is suggested as Al-Mn phase (average size about 5 μ m), with a portion of the non-passive manganese added to the Mg-Al matrix. The elongated grains (in gray) of several microns of the β -Mg₁₇Al₁₂ secondary phase were also observable. Studies have reported that Mn, as an alloying element, can promote an increase in corrosion resistance of Mg-Al alloys, reducing the metastable pit initiation in aluminum and decreasing the alloy anodic dissolution [55–58].

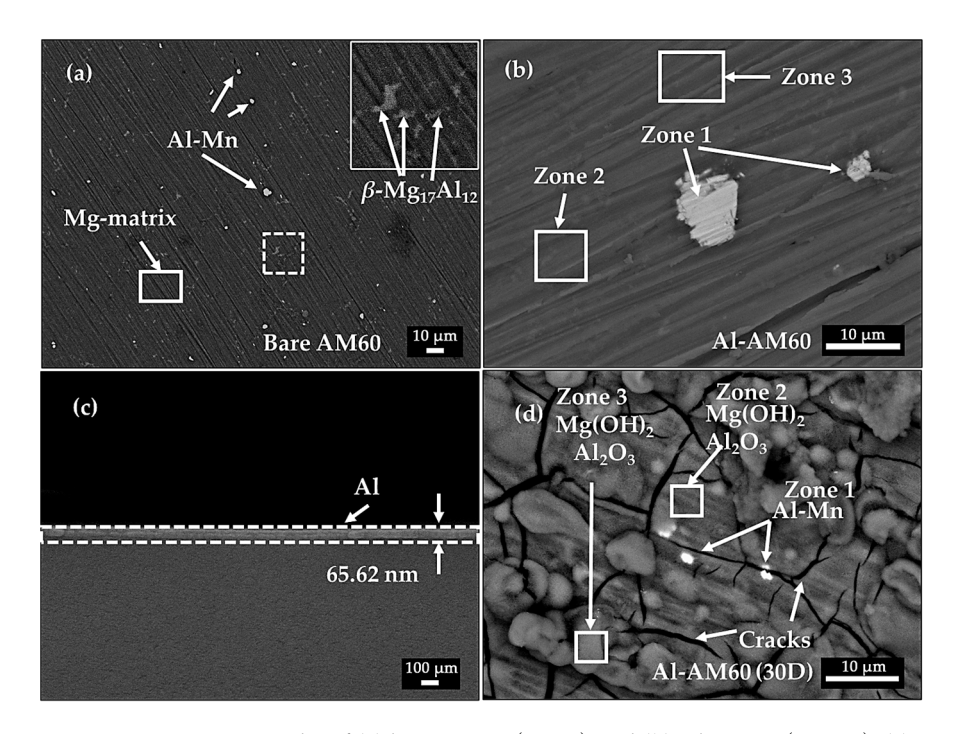


Figure 3. SEM micrographs of (**a**) bare AM60 (\times 500) and (**b**) Al-AM60 (\times 2000), (**c**) cross-section of Al-sputtered deposit (\times 20,000), and (**d**) Al-AM60 surface after 30 days of SME exposure (\times 2000).

Table 1. EDS elemental analysis (wt. %) of randomly selected surface areas (Figure 3) of the AM60 and Al-AM60 surfaces.

	Element	0	Mg	Al	Mn
	Al-Mn	2.52	26.26	34.17	37.05
AM60	Mg matrix	2.21	95.20	2.59	-
	β -Mg ₁₇ Al ₁₂	1.43	79.65	18.92	-
	Zone 1	5.67	3.56	38.88	51.89
Al-AM60	Zone 2	7.38	78.99	13.63	-
	Zone 3	5.49	81.86	12.65	-
Al-AM60 (30 days exposure)	Zone 1	45.06	21.43	18.55	14.96
	Zone 2	58.63	31.66	9.23	-
	Zone 3	64.68	28.21	6.70	-

In saline ambience, Mn at the surface may suffer selective dissolution, favoring the formation of a compacted protective layer of thinner surface aluminum oxide, enhancing the corrosion resistance of the alloy. After the modification of the AM60 surface by sputtered aluminum (Figure 3b, Table 1), it seems that the deposition of aluminum did not occur on the cluster surface of Al-Mn particles (Zone 1), but instead formed a thin film of ~ 65.62 nm

Coatings 2025, 15, 661 6 of 13

(Figure 3c) on the AM60 matrix, covering the microparticles of the β -Mg₁₇Al₁₂ secondary phase (Zones 2–3), presenting a stable deposition (~13.14 wt.%) in this area.

After 30 days of exposure to the saline model solution (SME), the Al-AM60 system exhibited significant changes in morphology and composition (Figure 3d, Table 1). The corrosion layer that developed on the surface presented visible cracks, and white particles related to the Al-Mn intermetallic were observable (Zone 1), which confirms their function as local cathodic sites in micro-galvanic pairs with the α -Mg phase (anodic active). Due to the immersion in SME solution, the AM60 alloy surface was subjected to degradation and formation of a corrosion layer of insoluble Mg(OH)₂. The evolution of bubbles of H₂ gas exerted pressure on the formed layer and caused micro-cracks:

$$Mg + 2H_2O \rightarrow Mg(OH)_2 + H_2$$
 (1)

EDS analysis suggested that the main corrosion product of the formed layer was $Mg(OH)_2$, enriched in Al and O (Al-oxide) (Zones 2 and 3) [59,60]. Because of the increase in pH (Equation (1)), it is considered that the surface of the metallic α -Al (reported by the XRD patterns, Figure 2) can suffer electrochemical oxidation to Al_2O_3 (Equation (2)) and its posterior dissolution (Equation (3)) consuming OH^- ions [59,60]:

$$2Al + 3H_2O \rightarrow Al_2O_3 + 6H^+ + 6e$$
 (2)

$$Al_2O_3 + 2OH^- \rightarrow AlO_{2 (aq)}^- + H_2O$$
 (3)

A corrosion study of AM50 specimens immersed for 96 h in aerated 1.6 wt%. NaCl (at room temperature) has reported that there are two parts in the formed corrosion layer: outer layer of amorphous MgO/Mg(OH)₂ and a thin inner layer of Al₂O₃ between metal and corrosion products [25,61]. EDS analysis has suggested that at the interface, an Al-rich layer exists, with a location-specific content, depend on the Al content during the solidification of the Mg-Al alloy and an accumulation of Al³⁺ [62]. This is because of the percolation of amorphous Al₂O₃ in MgO/Mg(OH)₂ corrosion layer [63], which improved the corrosion resistance of the alloy.

3.3. XPS Analysis of Al-AM60 Modified Alloy Surface

XPS analysis was performed in addition to XRD and SEM-EDS to verify the principal elements present on the Al-AM60 surface, as a part of the possible compounds. The high-resolution XPS spectra are shown in Figure 4.

The spectrum of Al2p (Figure 4a,d) was composed of two peaks with binding energy at ~72.58 eV attributed to the asymmetric metallic Al $2p_{3/2}$ peak (Al 0) and that at ~75.38 eV considered as characteristic of Al $^{3+}$ (Al $_2$ O $_3$) [64]. The energy separation between these Al2p peaks was estimated to be ~2.8 eV. After immersion for 30 days in the saline model solution (SME) the relative intensity of the Al-metallic peak was reduced by ~3 orders (Figure 4d) because of the reported electrochemical oxidation of the α -Al metallic phase (detected by XRD spectra) to Al $_2$ O $_3$ (Equation (2)) [59,60]. However, the peak of the formed Al $_2$ O $_3$ (at ~74.18 eV) still appeared on the Al-AM60 surface (Figure 4d) at lower intensity due to the suggested dissolution of this oxide (Equation (3)) to AlO $_2^-$ (aq). This way, the presence of the Al $_2$ O $_3$ content on the AM60 alloy favored the ~2.3 times reduced release of Mg $^{2+}$ ions (degradation of the Mg-matrix), and it is expected to provide protective layer [65]. On the other hand, the spectrum of O 1s (Figure 4b,e) displayed two peaks, at ~531.80 eV and at ~532.10 eV, commonly associated with the OH $^-$ ion [66]. The XPS analysis indicated that after immersion in the saline solution for 30 days, the peak intensity of the OH $^-$ ions increased trice, while that peak at ~531.80 eV was nearly constant. By relating the spectrum

Coatings 2025, 15, 661 7 of 13

of O 1s with that of Mg2p (Figure 4c,f) at ~50.58 eV of MgO and that of \sim 51.68 eV of Mg(OH)₂, it is observable that after immersion in the saline solution (SME), the intensity of the MgO diminished sharply, because it suffered corrosion and was gradually transformed to Mg(OH)₂ (Equation (1)).

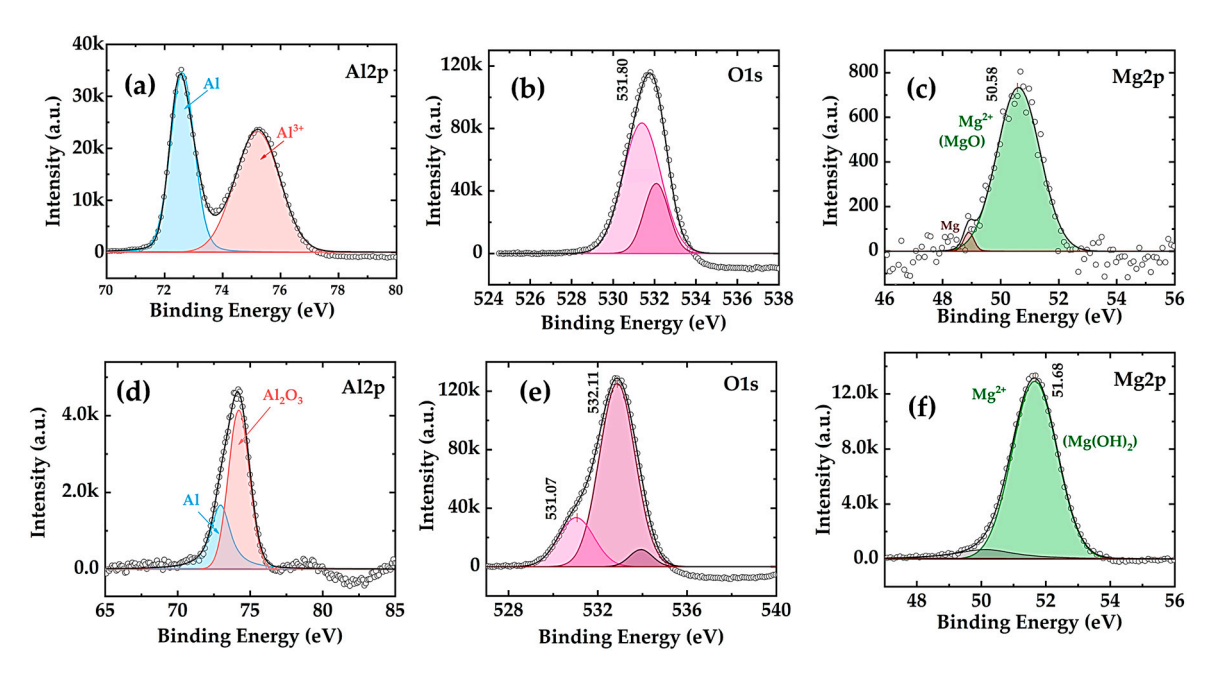


Figure 4. XPS high-resolution spectra peaks of Al 2p (a), O 1s (b), and Mg 2p (c) of Al-AM60 modified alloy surface, and spectra peaks of Al 2p (d), O 1s (e) spectrum of the deposited Al on AM60 magnesium alloy, (a) Al 2p peak, (b) O 1s peak, (c) Mg 2p peak and after 30 days of exposure to SME, (d) spectrum of Al 2p peak, (e) O 1s peak, and (f) Mg 2p peak.

3.4. Immersion Test in Model Saline Solution (SME)

Figure 5 compares the progress in time of pH of the saline model solution (SME) and ${\rm Mg^{2+}}$ ion release concentration (at 15 and 30 days) during the immersion of the studied uncoated AM60 and the modified surface of Al-AM60 alloys in SME; both parameters are indicators of the Mg-alloy degradation (electrochemical activity).

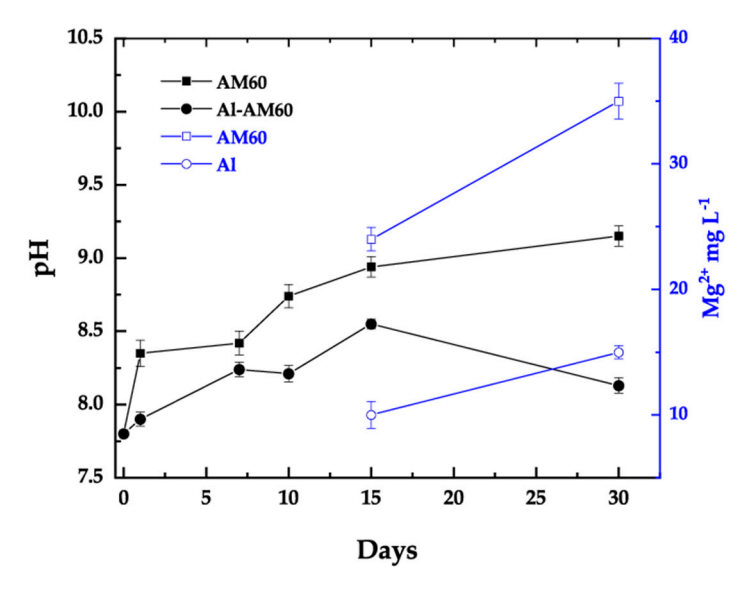


Figure 5. Change in time of SME marine solution pH (black line) and concentration of Mg^{2+} ion release (blue line) during immersion of uncoated AM60 and Al-AM60 alloys for 30 days in SME.

Coatings 2025, 15, 661 8 of 13

The microcracked first corrosion layer of insoluble $Mg(OH)_2$ (Figure 3d) was more susceptible to chloride ion (Cl⁻) penetration because of the H_2 evolution (Equation (1)) and posteriorly was transformed to the soluble corrosion product of $MgCl_2$:

$$Mg(OH)_2 + 2Cl^- \rightarrow MgCl_2 + 2OH^-$$
 (4)

This localized process is more accelerated around the micro-galvanic pairs of Al-Mn (cathodic active) in contact with the Mg-matrix (local anodes), leading to changes in the pH of the SME to more alkaline values. The change in pH values (Figure 5) indicated that this fact was less pronounced for the Al-AM60 (pH ≈ 8.13), in which the surface was modified with Al-sputtered nano-deposit, while the pH of the uncoated AM60 alloy reached a more alkaline value (~9.15), as an indication of a higher rate of electrochemical activity of the surface. The lower pH of the SME solution during the immersion of Al-AM60 can be attributed to the suggested electrochemical oxidation of aluminum to Al₂O₃ [25,59], which occurs with H⁺ formation and consumption of OH⁻ ions (Equations (2) and (3)). Notably, at the end of the immersion test, the Mg-ion release was significantly higher (~two times) for uncoated AM60 (35 mgL $^{-1}$), compared to that of Al-AM60 (15 mgL $^{-1}$). The lower ion release rate for Al-AM60 suggested that the presence of the nano-deposit of sputtered aluminum on the AM60 surface promoted a reduction of its electrochemical activity in the early stages. An explanation for this fact can be attributed to the studies [62,67] that have found an accumulation of $\mathrm{Al}^{3+}/\mathrm{AlO}_2^-$ species (Equation (3)) on the corroded surface because of the percolation of amorphous Al₂O₃ (Equation (2)) within the Mg/Mg(OH)₂ corrosion layer, improving the corrosion resistance of the alloy.

3.5. Electrochemical Tests

Figure 6 compares the change in time of the free corrosion potential (OCP) of the uncoated AM60 surface with that of Al-AM60, during their immersion in the model saline solution (SME). At 15 days the OCP of the Al-AM60 (modified with sputtered nano-deposit of aluminum) tended to a constant value of \sim 1.45 V, while the OCP of the uncoated AM60 maintained an increase over time, reaching \sim 1.52 V (more negative in \sim 70 mV), as an indicator of more active corrosion processes.

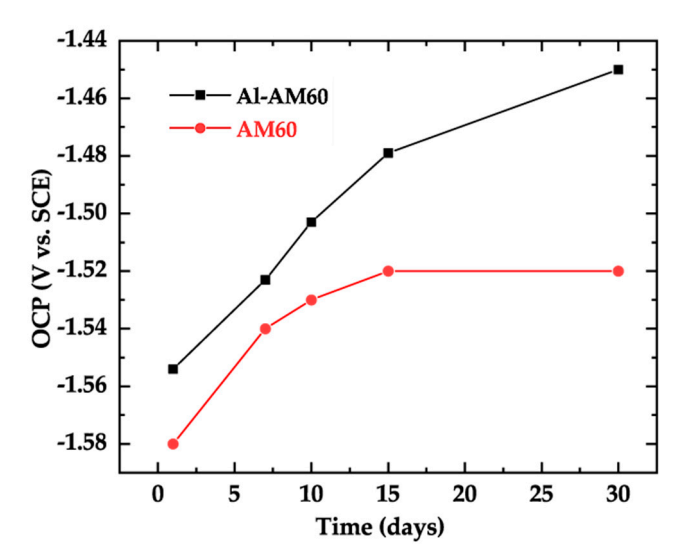


Figure 6. Change over time of the free corrosion potential (OCP) value of uncoated AM60 and Al-AM60 alloys during immersion in simulated marine solution (SME).

Figure 7 compares the Nyquist diagrams (Figure 7a) of uncoated AM60 and modified Al-AM60 surfaces, immersed for 7, 15, and 30 days to saline model solution (SME). The

Coatings 2025, 15, 661 9 of 13

Nyquist diagrams showed capacitive loops over the time of immersion; the characteristics were influenced by the changes that occurred at the interface alloy/SEM and influenced by the thickness and composition of the formed corrosion layer and mass/charge transport, as well as the existence of the Al-nano-deposit and the change in mass transport.

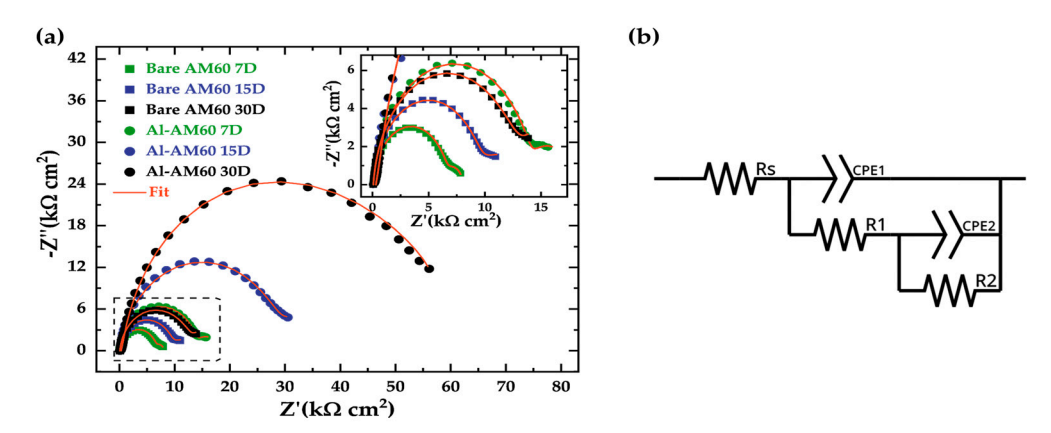


Figure 7. (a) Nyquist plots of EIS for 7, 15, and 30 days of exposure of bare (uncoated) AM60 and Al-AM60 after 30 days of immersion in SME solution, (b) equivalent circuit for fitting experimental EIS data.

As immersion time passed, the diameter of uncoated AM60 semi-circles was approximately thrice lower than those of the modified surface with Al-sputtered thin nano-deposit, indicating that the corrosion resistance of AM60 was improved significantly when exposed to simulated marine environment. The EIS data were fit to the equivalent circuit (Figure 7b) in our previous work for AM60 [46] and also reported in studies with EIS on Mg-alloys [68–71]. The main components are the following: Rs (electrolyte resistance); R_1 resistance and constant phase element (CPE₁) as "capacitance", used in parallel to model the behavior of a non-ideal capacitor, presenting the double layer at the metal/electrolyte interface, where species of different charge (Mg²⁺, Cl⁻ ions) at the electrolyte interface are transported through the formed layer of corrosion products and Al-deposit, acting as a physical barrier; R_2 (Rct) and CPE₂ "capacitance", introduced to characterize the charge transfer process of Mg²⁺ and H⁺ ions at the local anodic and cathodic sites of the alloy surface occurring through the MgO/Mg(OH)₂ layer. The obtained values of the alloy/electrolyte interface characteristic parameters are summarized in Table 2 (The circuit has a fitting of about 10^{-4}).

Table 2. Fitting parameters from EIS data of bare (uncoated) AM60 and Al-AM60 modified with sputtered Al-deposit film after immersion of 30 days in SME.

Rs (Ω cm ²)	CPE1 (μS s ⁿ cm ⁻²)	n1	R_1 (k Ω cm ²)	CPE2 (μS s ⁿ cm ⁻²)	n ²	R_2 (k Ω cm ²)	R_p (k Ω cm ²)			
AM60										
86.1 ± 0.44	60.65 ± 0.36	0.93 ± 0.03	12.85 ± 0.32	296.7 ± 0.40	0.71 ± 0.02	2.53 ± 0.21	15.46 ± 0.26			
Al-AM60										
89.6 ± 0.29	25.86 ± 1.34	0.87 ± 0.01	43.07 ± 1.20	11.29 ± 0.26	0.90 ± 0.01	12.87 ± 0.89	55.94 ± 1.04			

The overall polarization resistance expressed as $R_p=R_1+R_2$, was calculated to compare the electrochemical activity of the uncoated AM60 surface with that of modified Al-AM60 surface. The value of R_p (polarization resistance) was thrice higher for the corrosion process progress at the Al-AM60 modified surface (~55.94 k Ω cm²), compared to that of uncoated AM60 (~15.46 k Ω cm²). These facts coincided with the lower concertation of released Mg²+ ions from the Al-AM60 as a consequence of the hindered corrosion process

Coatings 2025, 15, 661 10 of 13

favored by the sputtered aluminum nano-deposit, providing a protective layer on the AM60 alloy surface exposed to a simulated marine environment (SME).

4. Conclusions

To achieve better corrosion resistance of AM60 (Mg-Al) alloy as engineering construction material, the surface was modified with DC magnetron sputtered aluminum nano-deposit (average thickness of \sim 65 nm). The sputtered Al film adhered to the α -Mg matrix where the particles of β -Mg₁₇Al₁₂ secondary phase were dispersed, while the Al-Mn intermetallic remained isolated. According to XPS analysis and XRD analysis, the aluminum nanofilm was composed of (111) and (200) crystal planes of the metallic aluminum metallic aluminum (Al⁰) and Al₂O₃ (Al³⁺). The initial stages of activity of uncoated AM60 and Al-AM60 surfaces were tested by immersion for 30 days in simulated saline solution (SME, pH 7.8). SEM-EDS analysis showed that due to the immersion in SME solution, the Mg-matrix surface of AM60 was subjected to degradation and microcracking (by H₂ bubble evolution), and the main corrosion product of the formed layer was Mg(OH)₂ enriched in Al and O (Al-oxide). The Al-AM60 maintained a lower alkaline value (pH~8.13) of SME, than that of the uncoated AM60 (pH~8.13), which was attributed to α -Mg electrochemical oxidation to Al₂O₃ and its posterior dissolution, consuming OH⁻ ions. Consequently, the concentration of the released Mg²⁺ ions from the Al-AM60 surface was reduced ~2.3 times (~15 mg L^{-1}) as an indication of the lower degradation rate. The Rp (polarization resistance), as inversely proportional to the corrosion current, was extracted from the EIS impedance data fitted to an equivalent electrical circuit. After 30 days in SME solution, the Rp value of the Al-AM60 modified surface was ~3.5 times higher than that of uncoated AM60 (15.46 k Ω cm²), confirming that the sputtered aluminum nano-deposit can hinder the corrosion process. The reported results might serve as a platform for further improvement in AM60 alloy corrosion resistance.

Author Contributions: G.S. performed the preparation of samples and the immersion tests; G.S. and E.F. contributed to the deposit sputtering methodology of the aluminum coating; G.S. and L.V. performed the formal analysis of the results and the writing of the original draft and its editing. L.V. supervised the project. All correspondence should be addressed to L.V. All authors have read and agreed to the published version of the manuscript.

Funding: This research received no external funding.

Institutional Review Board Statement: Not applicable.

Informed Consent Statement: Not applicable.

Data Availability Statement: The data are available upon request from the corresponding author.

Acknowledgments: Gerardo Sánchez acknowledges the Mexican Secretariat of Science, Humanities, Technology, and Innovation (SECIHTI) for the scholarship for his Ph.D. study. The authors gratefully thank the National Laboratory of Nano and Biomaterials (LANNBIO-CINVESTAV) for allowing the use of SEM-EDS, XPS, and XRD facilities; thanks also go to Victor Rejón, Daniel Aguilar, and Willian Cauich for their support in data acquisition.

Conflicts of Interest: The authors declare no conflicts of interest.

References

- Kojima, Y. Project of Platform Science and Technology for Advanced Magnesium Alloys. Mater. Trans. 2001, 42, 1154–1159.
 [CrossRef]
- 2. Pollock, T.M. Weight Loss with Magnesium Alloys. Science 2010, 328, 986–987. [CrossRef] [PubMed]
- 3. Panigrahi, S.K.; Kumar, K.; Kumar, N.; Yuan, W.; Mishra, R.S.; DeLorme, R.; Davis, B.; Howell, R.A.; Cho, K. Transition of Deformation Behavior in an Ultrafine Grained Magnesium Alloy. *Mater. Sci. Eng. A* **2012**, 549, 123–127. [CrossRef]

Coatings 2025, 15, 661 11 of 13

- 4. Luo, A.A. Magnesium Casting Technology for Structural Applications. J. Magnes. Alloys 2013, 1, 2–22. [CrossRef]
- 5. You, S.; Huang, Y.; Kainer, K.U.; Hort, N. Recent Research and Developments on Wrought Magnesium Alloys. *J. Magnes. Alloys* **2017**, *5*, 239–253. [CrossRef]
- 6. Cole, G.S. Issues That Influence Magnesium's Use in the Automotive Industry. Mater. Sci. Forum 2003, 419–422, 43–50. [CrossRef]
- 7. Polmear, I.J. Magnesium Alloys and Applications. Mater. Sci. Technol. 1994, 10, 1–16. [CrossRef]
- 8. Bai, J.; Yang, Y.; Wen, C.; Chen, J.; Zhou, G.; Jiang, B.; Peng, X.; Pan, F. Applications of Magnesium Alloys for Aerospace: A Review. *J. Magnes. Alloys* **2023**, *11*, 3609–3619. [CrossRef]
- 9. Aghion, E.; Bronfin, B. Magnesium Alloys Development towards the 21st Century. *Mater. Sci. Forum* **2000**, *350*–*351*, 19–30. [CrossRef]
- 10. Cole, G.S.; Sherman, A.M. Lightweight Materials for Automotive Application. *Mater. Charact.* 1995, 35, 3–9. [CrossRef]
- 11. Kulekci, M.K. Magnesium and Its Alloys Applications in Automotive Industry. *Int. J. Adv. Manuf. Technol.* **2008**, *39*, 851–865. [CrossRef]
- 12. Armao, F.G. Design & Fabrication of Aluminum Automobiles. Weld. Innov. 2002, 19, 2-6.
- 13. Powell, B.R.; Luo, A.A.; Krajewski, P.E. Magnesium Alloys for Lightweight Powertrains and Automotive Bodies. In *Advanced Materials in Automotive Engineering*; Rowe, J., Ed.; Woodhead Publishing: Sawston, UK, 2012; pp. 150–209. [CrossRef]
- 14. Zhang, W.; Xu, J. Advanced Lightweight Materials for Automobiles: A Review. Mater. Des. 2022, 221, 110994. [CrossRef]
- 15. Polmear, I.; Stjohn, D.; Nie, J.-F.; Qian, M. Magnesium Alloys. In *Light Alloys: Metallurgy of the Light Metals*; Garcia, A.C., Ed.; Butterworth-Heinemann: Oxford, UK, 2017; pp. 287–367. ISBN 978-0-08-099431-4.
- Kainer, K.U. The Current State of Technology and Potential for Further Development of Magnesium Applications. In Magnesium-Alloys and Technology; Kainer, K.U., Ed.; WILEY-VCH Verlag GmbH & Co. KGaA: Weinheim, Germany, 2003; pp. 1–22. ISBN 352730570X.
- 17. Makar, G.L.; Kruger, J. Corrosion of Magnesium. Int. Mater. Rev. 1993, 38, 138–153. [CrossRef]
- 18. Song, G.L.; Atrens, A. Corrosion Mechanisms of Magnesium Alloys. Adv. Eng. Mater. 1999, 1, 11–33. [CrossRef]
- 19. LeBozec, N.; Jönsson, M.; Thierry, D. Atmospheric Corrosion of Magnesium Alloys: Influence of Temperature, Relative Humidity, and Chloride Deposition. *Corrosion* **2004**, *60*, 356–361. [CrossRef]
- 20. Song, G.L.; St John, D.H.; Abbott, T. Corrosion Behaviour of a Pressure Die Cast Magnesium Alloy. *Int. J. Cast Met. Res.* **2005**, 18, 174–180. [CrossRef]
- 21. Jönsson, M. Atmospheric Corrosion of Magnesium Alloys: Influence of Microstructure and Environment. Ph.D. Thesis, School of Chemical Science and Engineering, KTH, Stockholm, Sweden, 2007.
- 22. Kainer, K.U.; Srinivasan, P.B.; Blawert, C.; Dietzel, W. Corrosion of Magnesium and Its Alloys. In *Shreir's Corrosion—Corrosion and Degradation of Engineering Materials*; Cottis, B., Graham, M., Lindsay, R., Lyon, S., Richardson, T., Scantlebury, D., Stott, H., Eds.; Elsevier: Amsterdam, The Netherlands, 2010; Volume 3, pp. 2011–2041. [CrossRef]
- 23. Liu, F.; Song, Y.; Shan, D.; Han, E.-H. Corrosion Mechanism of AM50 Magnesium Alloy in Simulated Acid Rain. *Recent Pat. Corros. Sci.* **2013**, *3*, 47–57. [CrossRef]
- 24. Esmaily, M.; Svensson, J.E.; Fajardo, S.; Birbilis, N.; Frankel, G.S.; Virtanen, S.; Arrabal, R.; Thomas, S.; Johansson, L.G. Fundamentals and Advances in Magnesium Alloy Corrosion. *Prog. Mater. Sci.* **2017**, *89*, 92–193. [CrossRef]
- 25. Danaie, M.; Asmussen, R.M.; Jakupi, P.; Shoesmith, D.W.; Botton, G.A. The Cathodic Behaviour of Al–Mn Precipitates during Atmospheric and Saline Aqueous Corrosion of a Sand-Cast AM50 Alloy. *Corros. Sci.* **2014**, *83*, 299–309. [CrossRef]
- 26. Blawert, C.; Dietzel, W.; Ghali, E.; Song, G. Anodizing Treatments for Magnesium Alloys and Their Effect on Corrosion Resistance in Various Environments. *Adv. Eng. Mater.* **2006**, *8*, 511–533. [CrossRef]
- 27. Ortiz, C.H.; Aperador, W.; Caicedo, J.C. Electrochemical Study of Anodized AZ31 Magnesium Alloy (Mg/MgO) Immersed under Watered Cementice Paste. *J. Mater. Eng. Perform.* **2022**, *31*, 8896–8905. [CrossRef]
- 28. Rahimian, M.; Parvin, N.; Ehsani, N. The Effect of Production Parameters on Microstructure and Wear Resistance of Powder Metallurgy Al–Al₂O₃ Composite. *Mater. Des.* **2011**, 32, 1031–1038. [CrossRef]
- 29. Li, Z.; Jing, X.; Yuan, Y.; Zhang, M. Composite Coatings on a Mg–Li Alloy Prepared by Combined Plasma Electrolytic Oxidation and Sol–Gel Techniques. *Corros. Sci.* **2012**, *63*, 358–366. [CrossRef]
- Salami, B.; Afshar, A.; Mazaheri, A. The Effect of Sodium Silicate Concentration on Microstructure and Corrosion Properties of MAO-Coated Magnesium Alloy AZ31 in Simulated Body Fluid. J. Magnes. Alloys 2014, 2, 72–77. [CrossRef]
- 31. Surmeneva, M.A.; Surmenev, R.A. Microstructure Characterization and Corrosion Behaviour of a Nano-Hydroxyapatite Coating Deposited on AZ31 Magnesium Alloy Using Radio Frequency Magnetron Sputtering. *Vacuum* **2015**, *117*, 60–62. [CrossRef]
- 32. Wu, H.; Qasim, A.M.; Xiao, S.; Huang, Q.; Zhang, F.; Wu, Z.; Fu, R.K.Y.; Wu, G.; Chu, P.K. Magnetron-Sputtered Fluorocarbon Polymeric Film on Magnesium for Corrosion Protection. *Surf. Coat. Technol.* **2018**, *352*, 437–444. [CrossRef]
- 33. Zhang, Z.; Kitada, A.; Fukami, K.; Murase, K. Aluminum Electroplating on AZ31 Magnesium Alloy with Acetic Anhydride Pretreatment. *Acta Metall. Sin.* **2022**, *35*, 1996–2006. [CrossRef]

Coatings 2025, 15, 661 12 of 13

34. Zhang, M.; Yu, X.; Sheng, M.; Chen, H.; Chen, B. Preparation of a Mussel-Inspired Supramolecular Polymer Coating Containing Graphene Oxide on Magnesium Alloys with Anti-Corrosion and Self-Healing Properties. *Int. J. Mol. Sci.* 2023, 24, 4981. [CrossRef]

- 35. Peng, F.; Li, H.; Wang, D.; Tian, P.; Tian, Y.; Yuan, G.; Xu, D.; Liu, X. Enhanced Corrosion Resistance and Biocompatibility of Magnesium Alloy by Mg-Al-Layered Double Hydroxide. *ACS Appl. Mater. Interfaces* **2016**, *8*, 35033–35044. [CrossRef]
- 36. Kumar, V.C.; Rajyalakshmi, G.; Kartha, J. Insights on Anti-Corrosion Coating of Magnesium Alloy: A Review. *J. Bio Tribo Corros*. **2023**, *9*, 1–21. [CrossRef]
- 37. Tan, J.; Liu, L.; Wang, H.; Luo, J. Advances in Anti-Corrosion Coatings on Magnesium Alloys and Their Preparation Methods. *J. Coat. Technol. Res.* **2024**, *21*, 811–825. [CrossRef]
- 38. Hoche, H.; Groß, S.; Oechsner, M. Development of New PVD Coatings for Magnesium Alloys with Improved Corrosion Properties. *Surf. Coat. Technol.* **2014**, 259, 102–108. [CrossRef]
- 39. Zhang, D.; Wei, B.; Wu, Z.; Qi, Z.; Wang, Z. A Comparative Study on the Corrosion Behaviour of Al, Ti, Zr and Hf Metallic Coatings Deposited on AZ91D Magnesium Alloys. *Surf. Coat. Technol.* **2016**, 303, 94–102. [CrossRef]
- 40. Carboneras, M.; López, M.D.; Rodrigo, P.; Campo, M.; Torres, B.; Otero, E.; Rams, J. Corrosion Behaviour of Thermally Sprayed Al and Al/SiCp Composite Coatings on ZE41 Magnesium Alloy in Chloride Medium. *Corros. Sci.* 2010, 52, 761–768. [CrossRef]
- 41. Tao, Y.; Xiong, T.; Sun, C.; Kong, L.; Cui, X.; Li, T.; Song, G.L. Microstructure and Corrosion Performance of a Cold Sprayed Aluminium Coating on AZ91D Magnesium Alloy. *Corros. Sci.* **2010**, *52*, 3191–3197. [CrossRef]
- 42. Yang, H.; Guo, X.; Wu, G.; Ding, W.; Birbilis, N. Electrodeposition of Chemically and Mechanically Protective Al-Coatings on AZ91D Mg Alloy. *Corros. Sci.* **2011**, *53*, 381–387. [CrossRef]
- 43. Sun, Z.; Zhang, D.; Yan, B.; Kong, D. Effects of Laser Remelting on Microstructures and Immersion Corrosion Performance of Arc Sprayed Al Coating in 3.5% NaCl Solution. *Opt. Laser Technol.* **2018**, *99*, 282–290. [CrossRef]
- 44. Liu, H.; Li, J.; Ma, D.; Jiang, X.; Xie, D.; Leng, Y. Influence of Interlayers on Adhesion Strength of TiN Film on Mg Alloy. *Coatings* **2024**, *14*, 121. [CrossRef]
- 45. Chávez, L.; Veleva, L.; Sánchez, G.; Dieringa, H. AM60-AlN Nanocomposite and AM60 Alloy Corrosion Activity in Simulated Marine-Coastal Ambience. *Metals* **2022**, *12*, 1997. [CrossRef]
- 46. Chávez, L.; Veleva, L.; Sánchez-Ahumada, D.; Ramírez-Bon, R. Hybrid Coating of Polystyrene–ZrO₂ for Corrosion Protection of AM Magnesium Alloys. *Coatings* **2023**, *13*, 1059. [CrossRef]
- 47. Sánchez, G.; Veleva, L.; Flores, E. Surface Modification of AM60 Mg-Al Alloy with Vanadium and V₂O₅ Sputtered Deposits: Activity in Marine Ambience. *Coatings* **2024**, *14*, 955. [CrossRef]
- 48. Chávez, L.; Veleva, L.; Castillo-Atoche, A. Electroless ZnO Deposition on Mg-Al Alloy for Improved Corrosion Resistance to Marine Environments. *Coatings* **2024**, *14*, 1192. [CrossRef]
- 49. *ASTM G31-21*; Standard Guide for Laboratory Immersion Corrosion Testing of Metals. ASTM International: West Con-shohocken, PA, USA, 2021.
- 50. Bedolla, E.; Lemus-Ruiz, J.; Contreras, A. Synthesis and Characterization of Mg-AZ91/AlN Composites. *Mater. Des.* **2012**, 38, 91–98. [CrossRef]
- 51. Esmaily, M.; Shahabi-Navid, M.; Mortazavi, N.; Svensson, J.E.; Halvarsson, M.; Wessén, M.; Jarfors, A.E.W.; Johansson, L.G. Microstructural Characterization of the Mg–Al Alloy AM50 Produced by a Newly Developed Rheo-Casting Process. *Mater. Charact.* **2014**, *95*, 50–64. [CrossRef]
- 52. Heczel, A.; Akbaripanah, F.; Salevati, M.A.; Mahmudi, R.; Vida; Gubicza, J. A Comparative Study on the Microstructural Evolution in AM60 Alloy Processed by ECAP and MDF. *J. Alloys Compd.* **2018**, 763, 629–637. [CrossRef]
- 53. Bu, H.; Yandouzi, M.; Lu, C.; Macdonald, D.; Jodoin, B. Cold Spray Blended Al+Mg₁₇Al₁₂ Coating for Corrosion Protection of AZ91D Magnesium Alloy. *Suf. Coat. Technol.* **2012**, 207, 155–162. [CrossRef]
- 54. Liu, Y.; Huang, J.; Claypool, J.; O'Keefe, M.J. Structure and Corrosion Behavior of Sputter Deposited Ce-Al-O Coating on Al 2024-T3 Alloy Substrate. *J. Electrochem. Soc.* **2016**, *163*, 198. [CrossRef]
- 55. Mraied, H.; Cai, W. The Effects of Mn Concentration on the Tribocorrosion Resistance of Al–Mn Alloys. *Wear* **2017**, 380–381, 191–202. [CrossRef]
- 56. Mraied, H.; Cai, W.; Sagüés, A.A. Corrosion Resistance of Al and Al-Mn Thin Films. Thin Solid Films 2016, 615, 391-401. [CrossRef]
- 57. Reffass, M.; Berziou, C.; Rébéré, C.; Billard, A.; Creus, J. Corrosion Behaviour of Magnetron-Sputtered Al_{1-x}–Mnx Coatings in Neutral Saline Solution. *Corros. Sci.* **2010**, *52*, 3615–3623. [CrossRef]
- 58. Chen, J.; Xiao, J.; Poplawsky, J.; Michel, F.M.; Deng, C.; Cai, W. The Origin of Passivity in Aluminum-Manganese Solid Solutions. *Corros. Sci.* **2020**, 173, 108749. [CrossRef]
- 59. Moon, S.M.; Pyun, S.I. The Corrosion of Pure Aluminium during Cathodic Polarization in Aqueous Solutions. *Corros. Sci.* **1997**, 39, 399–408. [CrossRef]
- 60. Van de Ven, E.P.G.T.; Koelmans, H. The Cathodic Corrosion of Aluminum. J. Elchem. Soc. 1976, 123, 143–145. [CrossRef]
- 61. Asmussen, R.M.; Binns, W.J.; Partovi-Nia, R.; Jakupi, P.; Shoesmith, D.W. The Stability of Aluminum-Manganese Intermetallic Phases under the Microgalvanic Coupling Conditions Anticipated in Magnesium Alloys. *Mater. Corros.* **2016**, *67*, 39–50. [CrossRef]

Coatings 2025, 15, 661 13 of 13

62. Wang, L.; Shinohara, T.; Zhang, B.P. XPS Study of the Surface Chemistry on AZ31 and AZ91 Magnesium Alloys in Dilute NaCl Solution. *Appl. Surf. Sci.* **2010**, 256, 5807–5812. [CrossRef]

- 63. Zähr, J.; Oswald, S.; Türpe, M.; Ullrich, H.J.; Füssel, U. Characterisation of Oxide and Hydroxide Layers on Technical Aluminum Materials Using XPS. *Vacuum* **2012**, *86*, 1216–1219. [CrossRef]
- 64. Zhou, W.; Xue, F.; Li, M. Corrosion Behavior of Al-Mg Alloys with Different Alloying Element Contents in 3.5% NaCl Solution. *Metals* **2025**, *15*, 327. [CrossRef]
- 65. Kloprogge, J.T.; Duong, L.V.; Wood, B.J.; Frost, R.L. XPS Study of the Major Minerals in Bauxite: Gibbsite, Bayerite and (Pseudo-) Boehmite. *J. Colloid Interface Sci.* **2006**, 296, 572–576. [CrossRef]
- 66. Esfandiari, N.; Aliofkhazraei, M.; Colli, A.N.; Walsh, F.C.; Cherevko, S.; Kibler, L.A.; Elnagar, M.M.; Lund, P.D.; Zhang, D.; Omanovic, S.; et al. Metal-Based Cathodes for Hydrogen Production by Alkaline Water Electrolysis: Review of Materials, Degradation Mechanism, and Durability Tests. *Prog. Mater. Sci.* 2024, 144, 101254. [CrossRef]
- 67. Nordlien, J.H.; NişancioĞu, K.; Ono, S.; Masuko, N. Morphology and Structure of Oxide Films Formed on MgAl Alloys by Exposure to Air and Water. *J. Electrochem. Soc.* **1996**, 143, 2564–2572. [CrossRef]
- 68. Delgado, M.C.; García-Galvan, F.R.; Barranco, V.; Feliu, S. A Measuring Approach to Asses the Corrosion Rate of Magnesium Alloys Using Electrochemical Impedance Spectroscopy. In *Magnesium Alloys*; Aliofkhazraei, M., Ed.; IntechOpen: Rijeka, Croatia, 2017; pp. 129–160. [CrossRef]
- 69. Shkirskiy, V.; King, A.D.; Gharbi, O.; Volovitch, P.; Scully, J.R.; Ogle, K.; Birbilis, N. Revisiting the Electrochemical Impedance Spectroscopy of Magnesium with Online Inductively Coupled Plasma Atomic Emission Spectroscopy. *ChemPhysChem* **2015**, 16, 536–539. [CrossRef] [PubMed]
- 70. Curioni, M.; Scenini, F.; Monetta, T.; Bellucci, F. Correlation between Electrochemical Impedance Measurements and Corrosion Rate of Magnesium Investigated by Real-Time Hydrogen Measurement and Optical Imaging. *Electrochim. Acta* 2015, 166, 372–384. [CrossRef]
- 71. Brooks, E.K.; Der, S.; Ehrensberger, M.T. Corrosion and Mechanical Performance of AZ91 Exposed to Simulated Inflammatory Conditions. *Mater. Sci. Eng. C* **2016**, *60*, 427–436. [CrossRef]

Disclaimer/Publisher's Note: The statements, opinions and data contained in all publications are solely those of the individual author(s) and contributor(s) and not of MDPI and/or the editor(s). MDPI and/or the editor(s) disclaim responsibility for any injury to people or property resulting from any ideas, methods, instructions or products referred to in the content.